New Mexico Geological Society

Downloaded from: https://nmgs.nmt.edu/publications/guidebooks/76



Landslides Along the Southernmost West Mesa Escarpment, Petroglyph National Monument, Albuquerque, New Mexico

William C. Haneberg and Sean D. Connell
2026, pp. 291-300. https://doi.org/10.56577/FFC-76.291

in:

Geology of the Albuquerque Region - Fall Field Conference 2026, Connell, Sean D.; Koning, Daniel J.;, New Mexico Geological Society 76th Annual Fall Field Conference Guidebook, 452 p. https://doi.org/10.56577/FFC-76

This is one of many related papers that were included in the 2026 NMGS Fall Field Conference Guidebook.

Annual NMGS Fall Field Conference Guidebooks

Every fall since 1950, the New Mexico Geological Society (NMGS) has held an annual Fall Field Conference that explores some region of New Mexico (or surrounding states). Always well attended, these conferences provide a guidebook to participants. Besides detailed road logs, the guidebooks contain many well written, edited, and peer-reviewed geoscience papers. These books have set the national standard for geologic guidebooks and are an essential geologic reference for anyone working in or around New Mexico.

Free Downloads

NMGS has decided to make peer-reviewed papers from our Fall Field Conference guidebooks available for free download. This is in keeping with our mission of promoting interest, research, and cooperation regarding geology in New Mexico. However, guidebook sales represent a significant proportion of our operating budget. Therefore, only *research papers* are available for download. *Road logs*, *mini-papers*, and other selected content are available only in print for recent guidebooks.

Copyright Information

Publications of the New Mexico Geological Society, printed and electronic, are protected by the copyright laws of the United States. No material from the NMGS website, or printed and electronic publications, may be reprinted or redistributed without NMGS permission. Contact us for permission to reprint portions of any of our publications.

One printed copy of any materials from the NMGS website or our print and electronic publications may be made for individual use without our permission. Teachers and students may make unlimited copies for educational use. Any other use of these materials requires explicit permission.

This page is intentionally left blank to maintain order of facing pages.

New Mexico Geological Society Guidebook, 76th Fall Field Conference, 2026, p. 291–300, https://doi.org/10.56577/FFC-76.291

LANDSLIDES ALONG THE SOUTHERNMOST WEST MESA ESCARPMENT, PETROGLYPH NATIONAL MONUMENT, ALBUQUERQUE, NEW MEXICO

WILLIAM C. HANEBERG[1] AND SEAN D. CONNELL[2]

[1]Geological and Geohazards Consultant, Albuquerque, NM 87120; bill@haneberg.com
[2]New Mexico Bureau of Geology and Mineral Resources, Socorro, NM 87801

Abstract—The geomorphology of the southernmost West Mesa escarpment (SWME), which is aligned with a known down-to-the-east middle to late Quaternary normal fault as inferred from borehole and aeromagnetic information, is noticeably different than that of the rest of the 28-km (17-mi) long escarpment. In addition to having an unusually straight and nearly north-south trace, the SWME includes a 1-km (0.6 mi) long zone of previously undocumented basalt-capped rotational (Toreva block) landslides characterized by arcuate scarps and concave headwalls, tilted strata, bulked convex toes, and slope profiles suggesting at least one and perhaps two episodes of retrogressive movement. The SWME is the only portion of the West Mesa escarpment with significant landslides. The landslides do not appear to be active. Geomorphometric maps derived from airborne lidar digital elevation models additionally show that the SWME is rougher and has more highly disrupted drainage than portions of the escarpment that are not coincident with the fault. The absolute ages of the landslides are unknown; however, the relative ages of the Albuquerque Volcanoes basalt flows and the fault may preclude the possibility that the SWME is a simple down-to-the-east normal fault scarp degraded by landslides. One possible explanation is that flowing basalt was blocked by a north-south obsequent fault-line scarp with landslides occurring after topographic inversion. This model suggests that footwall sediments were removed by erosion along an ancestral arroyo ultimately draining eastward, creating the relief necessary for the landslides to occur, perhaps in response to the late Pleistocene pluvial conditions and base-level adjustment along the Rio Grande. Probabilistic slope stability simulations suggest that initial vertical slopes are likely to be unstable under dry conditions, and that groundwater, if present, would decrease the stability of the escarpment.

INTRODUCTION

The West Mesa escarpment is, after the Albuquerque Volcanoes, the most prominent geomorphological feature on Albuquerque's west side. The 50-m (164-ft) high escarpment, which falls within the Petroglyph National Monument, is along most of its 28 km (17 mi) length an anastomosing landform characterized by geologically unremarkable colluvial slopes covered with culturally significant petroglyph-bearing basalt boulders (Fig. 1). The southernmost kilometer of the West Mesa escarpment—which we refer to as the SWME in this paper—is distinctive because it is both strikingly straight compared to the rest of the escarpment and aligned with the projection of a concealed north-south striking fault identified from aeromagnetic surveys (Grauch et al., 2001; Sweeney et al., 2002; Shroba et al., 2003; Connell, 2008). The SWME is also the only portion of the escarpment along which large rotational landslides—documented for the first time in this paper—have occurred. Although the landslides have not previously been recognized as such, they have been described as "natural terraces" used for agriculture and grazing in historic and prehistoric times, and which are associated with petroglyph concentrations (NPS, 1991).

The combination of unusual straightness, alignment with an inferred fault having no other surface expression, and landslides suggests that the geologic history of the SWME is different, and we think more interesting, than the rest of the escarpment.

The SWME lies within the Petroglyph National Monument and is most easily accessed via the South Point Day

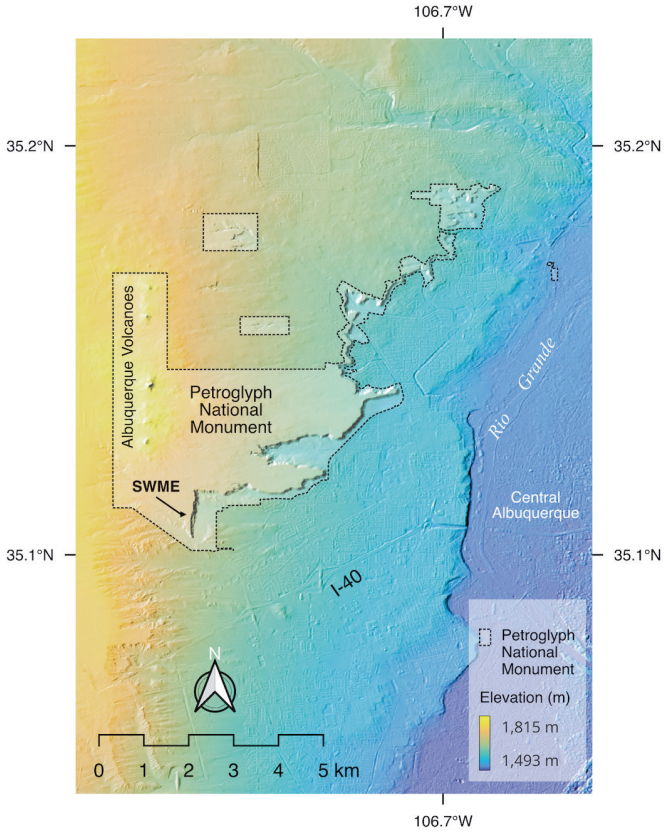


FIGURE 1. Topographic shaded relief image showing the location of the Petroglyph National Monument, the Southernmost West Mesa escarpment (SWME), and other prominent features. Elevation data source: U.S. Geological Survey.

Use Area trailhead (WGS84 GPS coordinates: N35.10140°, W106.75506°). Follow the trail from the southwestern corner of the parking lot parallel to the Monument boundary fence until you reach a pedestrian gate about 100 m (328 ft) from the parking lot. Pass through the gate and walk about 400 m (1,312 ft) before bearing right at a trail junction just past a small arroyo. Continue another 300 m (984 ft), crossing a larger arroyo before reaching South Point, where an unsigned trail runs along the base of the escarpment. Return via the same route. Obey the signs and do not cross into areas marked off-limits. The day-use area parking lot has pit toilets but no water or shade.

GEOLOGIC SETTING

The SWME is within the La Mesita Negra SE 7.5-minute geologic quadrangle mapped by Shroba et al. (2003) and, more broadly, among a series of down-to-the-east normal faults that mark the western margin of a graben identified by Connell (2008). Figure 2 is a geologic map of the SWME and surrounding areas produced using GIS polygon and line data from Connell (2006) and stratigraphic terminology from Connell (2008), draped over a regional lidar hillshade image to illustrate the local topography. The escarpment slopes are mapped as Holocene to middle(?) Pleistocene colluvium developed on undivided Pliocene to middle Miocene Santa Fe Group sediments by Shroba et al. (2003) and colluvium and alluvium (undivided) developed on lower Pleistocene(?) to Pliocene cobbly sands and gravels of the Rio Puerco Member of the Ceja Formation by Connell (Connell, 2008; Connell et al., 2013). Kelley (1977) previously mapped the escarpment as the Ceja Member of the Santa Fe Group and did not show any colluvium.

The escarpment is capped by a series of five thin, middle Pleistocene basaltic lava flows emanating from the Albuquerque Volcanoes and which flowed mostly eastward down the gently sloping Llano de Albuquerque (Kelley, 1977). Singer et al. (2008) and Peate et al. (1996) reported 218±14 ka and 156±20 ka dates from $^{40}Ar/^{39}Ar$ and $^{238}U/^{230}Th$ analyses, respectively. The flows are covered in some places by older and younger Quaternary alluvium and undivided Quaternary alluvium and colluvium (Shroba et al., 2003; Connell, 2008). East of the SWME, topographically prominent erosional remnants of the Rio Puerco Member, surrounded by alluvial and eolian deposits, provide evidence of post-volcanic topographic inversion. Ceja Formation erosional remnants locally have about one-third to one-half the relief of the escarpment.

High-resolution aeromagnetic surveys of the Albuquerque Basin provide evidence of numerous concealed faults in the vicinity of the monument (Grauch et al., 1999). Surficial geologic mapping by Shroba et al. (2003) and Connell (2008) both interpret a linear aeromagnetic anomaly along

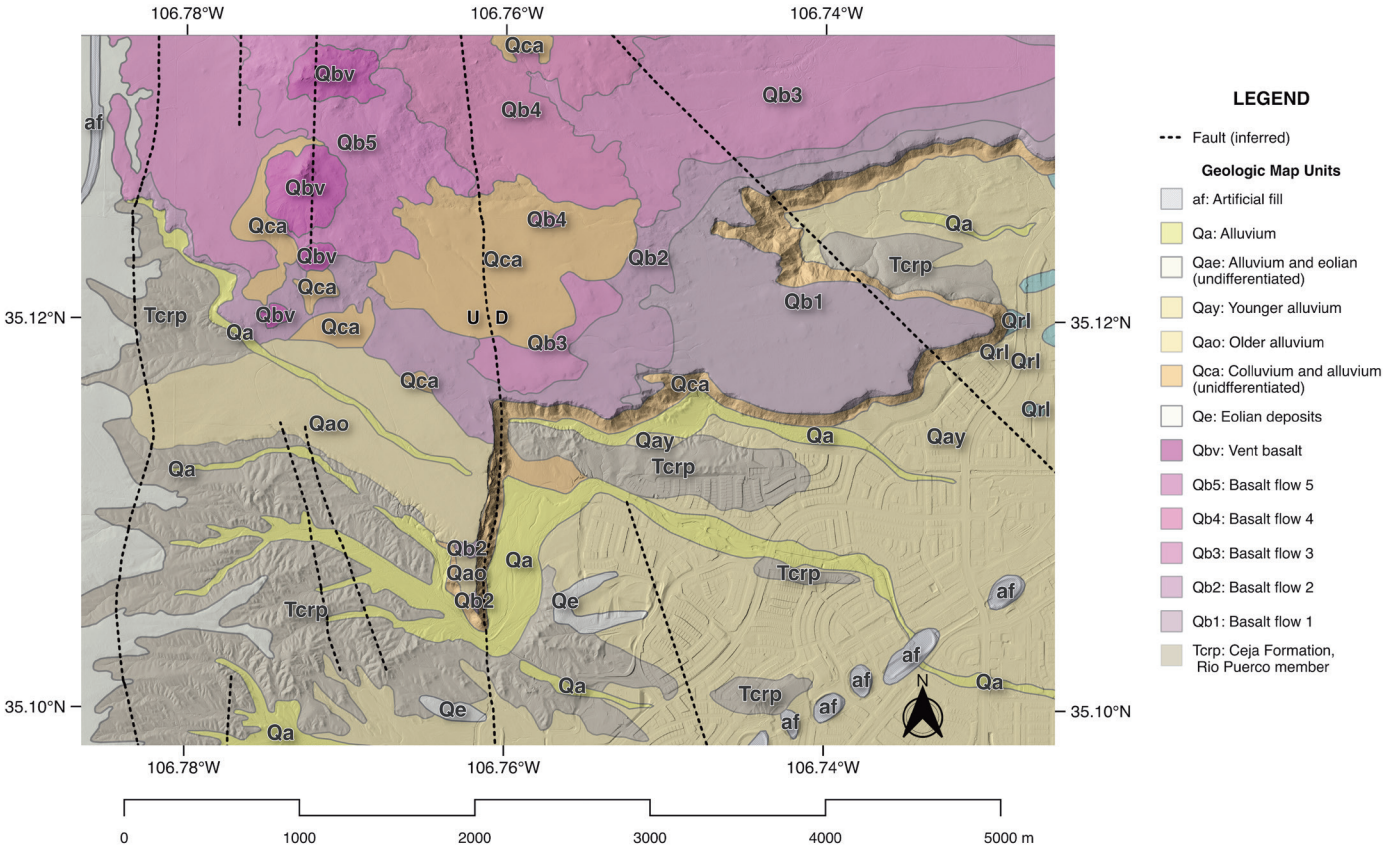


FIGURE 2. Geologic map of the SWME and surrounding area draped over a lidar multidirectional hillshade image. Geologic polygon and line data from Connell (2006) revised to conform with the nomenclature of Connell (2008). Lidar coverage courtesy of the Mid-Region Council of Governments.

the SWME as a normal fault. The Ceja Formation is poorly exposed south of the Albuquerque Volcanoes, which hampers the determination of relative vertical movement. Shroba et al. (2003) interpret this feature to have down-to-the-west relative vertical separation, whereas Connell (2008) interpreted down-to-the-east separation based on correlations of subsurface stratigraphic markers in nearby wells. For example, the Don #1 well was interpreted to have been drilled into a buried horst block approximately 3.6 km (2.2 mi) south of the southern tip of the SWME. Geologic cross-section C–C' of Connell (2008) is approximately 1.3 km (0.8 mi) south of the escarpment. Along this cross section, the Atrisco Member of the Ceja Formation displays minimal (<10 m [33 ft]) of vertical separation across a down-to-the-west fault located <0.3 km (0.2 mi) west of the Don #1 well. Less than 0.2 km (0.1 mi) east of the Don #1 well, the Atrisco Member is offset by approximately 75 m (246 ft) in a down-to-the-east sense. Shroba et al. (2003) did not provide cross sections, so it is difficult to verify their interpretation. We use the Connell (2008) interpretation in this paper because, in our opinion, it is based on the best available information. Personius and Jochems (2016) assigned a middle to late Quaternary (<750 ka) age of last movement to the fault while noting that at least two nearby N–S faults offset the Albuquerque Volcanoes basalt. Deposition of the Ceja Formation may have ceased shortly after ~1.8 Ma (Connell et al., 2013), indicating that the late Quaternary fault assessment of Personius and Jochems (2016) may be older by a factor of 2.4.

Neither Kelley (1977), Shroba et al. (2003), nor Connell (2008) show landslides along the SWME on their maps. An erosion assessment report (Gellis, 1995) notes one landslide in the Boca Negra Canyon portion of the monument, several kilometers north of the SWME, along with evidence of significant erosion on the mesa and a gully at the northern end of the SWME, but does not describe landslides along the SWME.

Santa Fe Group strata—including the Ceja Formation—are described by many geologists as unconsolidated or weakly consolidated. The term consolidation, however, is used differently in soil mechanics. These strata are, in a soil-mechanics sense, over-consolidated—not unconsolidated—by virtue of fluvial incision along the Rio Grande valley along the basin axis and tectonic exhumation along the basin flanks. Geophysical-log-derived elastic moduli for Santa Fe Group strata are typical of weak sedimentary rocks (Haneberg, 1999).

METHODS

Our work involved qualitative observations from established trails during numerous visits to the Monument between 2023 and 2025, digital terrain analysis of publicly available airborne lidar data, and a series of exploratory probabilistic slope stability analyses to better understand conditions that may have contributed to landslides along the SWME.

The airborne lidar data are from a 2018 survey conducted by the surveying firm Atlantic on behalf of the Mid-Region Council of Governments (MRCOG), with a nominal pulse spacing of 0.49 m (1.62 ft) and a final digital elevation model (DEM) grid spacing of 0.61 m (2 ft). The lidar project report (Atlantic, 2018) contains complete metadata and accuracy verification statistics. We chose to work with gridded DEMs rather than point cloud data to simplify lidar derivative map computations, which are most easily performed on a regular grid, and because there is little difference between the nominal point cloud pulse spacing and the final DEM grid spacing.

We obtained lidar data in 1,350-by-1,350-cell GeoTIFF files covering the project area and produced a merged 0.61-m (2-ft) DEM for the area shown in Figure 2. From the DEM, we further produced a series of derivative maps to support geomorphological and engineering geological interpretation of the SWME using the open-source GIS software QGIS. The derivative maps included a multi-directional hillshade, slope angle, 51-cell moving window residual topography defined as the difference between the original DEM and a 51-cell moving average DEM (Johnson and Haneberg, 2025), and topographic roughness calculated as the 51-cell moving window standard deviation of the slope angle (Grohmann et al., 2011). Slope-shade maps, which are slope-angle maps with a light-to-dark color ramp, accentuate features such as landslide scarps and toes. Different moving window sizes will accentuate different scales of landscape variability (Johnson and Haneberg, 2025), and should be chosen with an understanding of the scale of the landforms to be highlighted. For this paper, we chose 51-cell moving windows based on the ~80 m (~250 ft) to ~120 m (~400 ft) map-view width of the SWME slope. This allowed moving-window calculations near the mid-point of the SWME slope to sample values over much of the slope width without including too many values from flat areas adjacent to the SWME slope.

To better understand potential contributions of precipitation on slope stability, we calculated a flow accumulation map by aggregating the original 0.61-m (2-ft) DEM to a coarser 15.24-m (50-ft) DEM, ensuring hydrologic continuity by applying a least-cost breaching algorithm (Lindsay and Dhun, 2015), and running a D-infinity (Tarboton, 1997) flow routing algorithm as implemented in the Whitebox Tools geomorphological analysis toolkit (Lindsay, 2016) to show the total upslope contributing area for each DEM cell. The map serves as a proxy for the ability of the watershed to deliver groundwater or surface water to the landslide locations.

In addition to the lidar derivative maps, we extracted and plotted 8 topographic profiles across the landslide-prone SWME and an adjacent portion of the escarpment without known landslides to document the landslide topography.

Finally, we undertook a series of slope stability simulations to better understand the influence of initial slope geometry and subsurface water on the origin of the SWME landslides using our own probabilistic implementation of Bishop's (1955) method to calculate factors of safety against sliding for vertical and non-vertical slopes. The factor of safety, F, is the ratio of the resisting to the driving moments in the slope, developed around a center of rotation defining a circular potential slip surface. Values of $F \geq 1$ indicate that the resisting moment equals or exceeds the driving moment and the slope should be stable; values of $F < 1$ indicate the obverse and the slope should be unstable. Following the example of Dortch et al. (2009), we

used a generic pore-water pressure coefficient, r_u, which is the ratio of pore-water pressure to lithostatic pressure within the slope. A value of $r_u = 0$ indicates zero pore water pressure (i.e., a dry slope). A value of $r_u = 1$ indicates that pore-water pressure equals lithostatic pressure, which is unlikely to occur except in over-pressured sedimentary basins. A slope saturated to the ground surface under hydrostatic conditions would, given typical densities of earth materials and water, have a value of $r_u \approx 0.5$. The benefit of the r_u approach in paleo-landslide studies (e.g., Dortch et al., 2009) is that it allows us to incorporate potential effects of pore-water pressure without specifying details of an unknown paleo-groundwater flow system.

While Bishop's (1955) method is not as sophisticated as some approaches, it is robust in its simplicity, requires few parameters, and is useful for back-of-the-envelope comparisons of conceptual models in situations where few data are available. We performed iterative Monte Carlo simulations (100,000 iterations each) to account for parameter uncertainty, yielding probability distributions and estimates of the probability that $F < 1$, rather than single factor-of-safety values, for each of our idealized slopes.

RESULTS

Slope Morphology

The landslides along the SWME are characterized by hummocky terrain including vertical headscarps developed in basalt flows at the top of the escarpment, horizontal to gently tilted flat areas delineating the tops of multiple slide blocks, and convex toes distinct from the colluvial slopes along the rest of the escarpment (Fig. 3). The landslide and colluvial slopes are both covered with angular to sub-angular basalt boulders ranging from about 1–3 m (3.3–9.8 ft) in diameter, with no evidence of basalt boulders beyond the current margin of the escarpment (implying that basalt did not flow beyond the escarpment and that the escarpment has not retreated since the flows occurred). There are no seeps or springs—nor evidence of past significant seepage, such as travertine or tufa deposits—visible along the SWME. There are no indications that the landslides are currently active. However, numerous small alluvial fans composed of fine- to coarse-grained sand and pebbles occur along the landslide toes.

Figure 4 illustrates four ways to visualize and quantify the geomorphology of the SWME slope using the publicly available lidar data: a multi-directional hillshade image, a slope-shade map, a residual topography map, and a topographic roughness map. Both the hillshade and slope-shade maps show easily recognized landslide features in map view, including broadly arcuate headscarps, flat to slightly tilted areas separated by internal scarps, and bulging landslide toes along the southern three-quarters of the SWME. The residual topography map, which highlights local topographic highs and lows relative to a smoothed elevation surface, shows the same landslide-prone portion of the SWME to be characterized by a poorly integrated channel network, in contrast to well-integrated channel networks on adjacent undeformed colluvial slopes and Ceja Formation erosional remnants. The topographic roughness

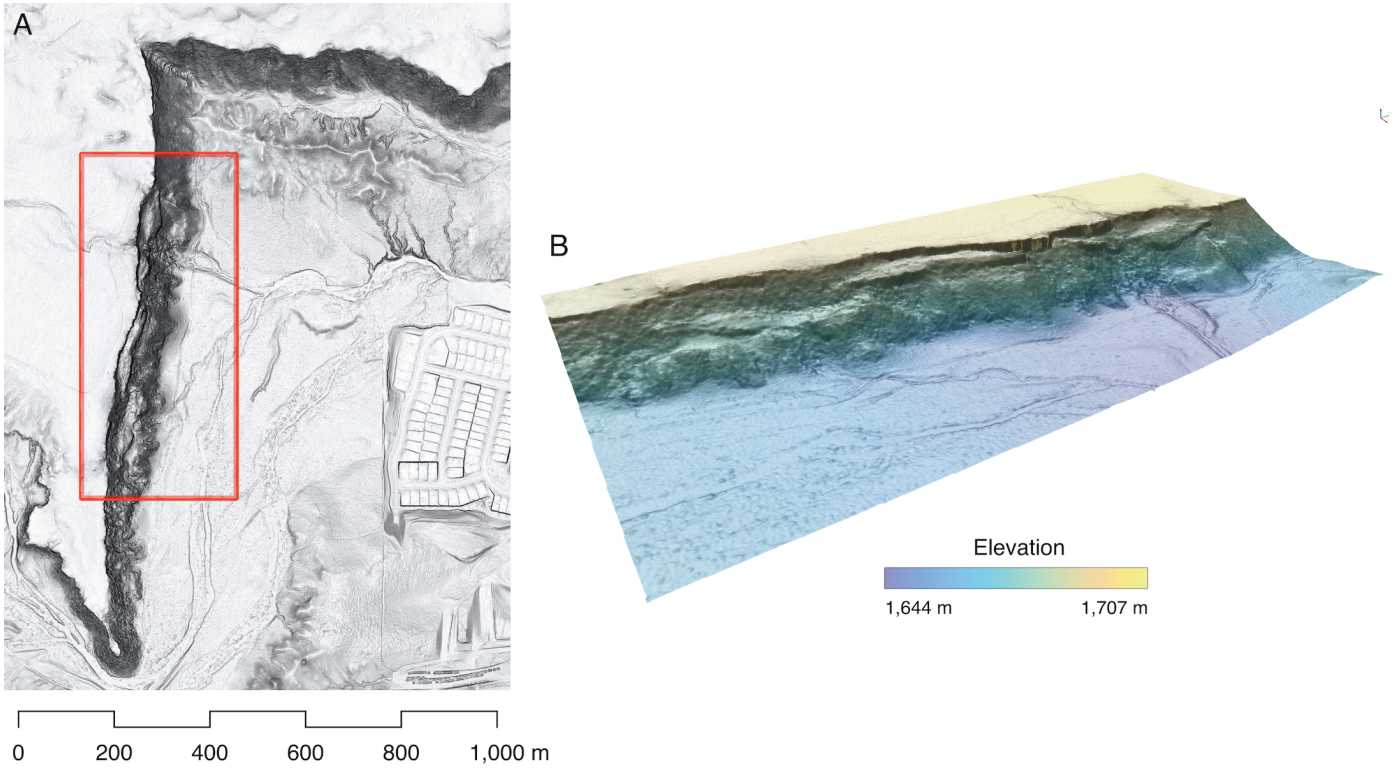


FIGURE 3. A) Lidar-derived slope-shade map of the SWME and adjoining areas illustrating landslide-related landforms. Light shades indicate gentle slopes and dark shades indicate steep slopes. B) 3-D perspective view of a lidar slope-shade map covering the red boxed area in 3A, colored according to elevation and illustrating the same landslide features.

map shows that the landslide-prone portion of the SWME is conspicuously rougher than the adjacent colluvial slopes. Both the degree of channel network disorganization and topographic roughness increase northward along the SWME, reaching a point where the SWME is currently adjacent to a prominent erosional remnant of the Ceja Formation. North of this point, there are no obvious landslide features, the degree of channel system integration increases, and the topographic roughness decreases to levels consistent with the rest of the escarpment. Topographic profiles extracted from the lidar DEM also show distinct differences between the landslide-prone portion of the SWME and undeformed colluvial slopes consistent with the hillshade, slope-shade, residual topography, and topographic roughness maps (Fig. 5).

Our surface-water flow accumulation results show that the total contributing area along the top of the SWME ranges from 234 m^2 (2,519 ft^2) to 2.6 km^2 (1.00 mi^2) at a point just above the highest concentration of landslides (Fig. 6). We used log-transformed units in Figure 6 to best visualize the full range of values within the model domain. A second, more diffuse accumulation path, about 300 m (1,000 ft) south and also above the highest concentration of landslides, has a calculated contributing area greater than 0.31 km^2 (0.12 mi^2). The highest calculated flow accumulation value, which occurs downstream of the SWME, is 7.1 km^2 (2.74 mi^2).

Other less developed flowpaths crossing the SWME above the landslides drain areas on the order of 0.1 km^2 (0.04 mi^2), suggesting a total contributing area greater than 3 km^2 (1.16 mi^2). That is appreciably greater than other portions of the West Mesa escarpment that are not characterized by landslides.

Slope-Stability Simulations

We evaluated four highly idealized hypothetical slopes to gain insight into the origin of the SWME landslides: vertical and non-vertical initial slopes under both dry and wet conditions. We assumed, based on the requirements of Bishop's (1955) method, that the simulated slip surfaces were circular arcs and, from our field observations, vertical at the top of the 50-m high escarpment (Fig. 7). There are no known published geotechnical property data relevant to slope stability analyses for the Ceja Formation in the vicinity of the SWME, so we heuristically inferred physically plausible normal (Gaussian) input probability distributions for both the basalt caprock and Ceja Formation sedimentary strata based on our engineering geological experience (Table 1). We assumed that headscarps in the basalt caprock would develop along existing joints with frictional but no cohesive strength.

Our probabilistic simulations produced symmetric distributions with mean-to-median ratios of 1.00 and small standard deviations (Fig. 8 and Table 2). The results suggest that vertical slopes in over-consolidated Ceja Formation strata capped by basalt are unstable under dry, let alone wet conditions. Non-vertical dry slopes, in comparison, are remarkably stable.

TABLE 1. Means and standard deviations of parameters for probabilistic slope stability simulations.

Unit	Density (kg/m^3)	Cohesion (kPa)	Friction Angle
Basalt	2900 ± 50	0 ± 0	35 ± 2°
Ceja	1900 ± 50	100 ± 10	35 ± 2°

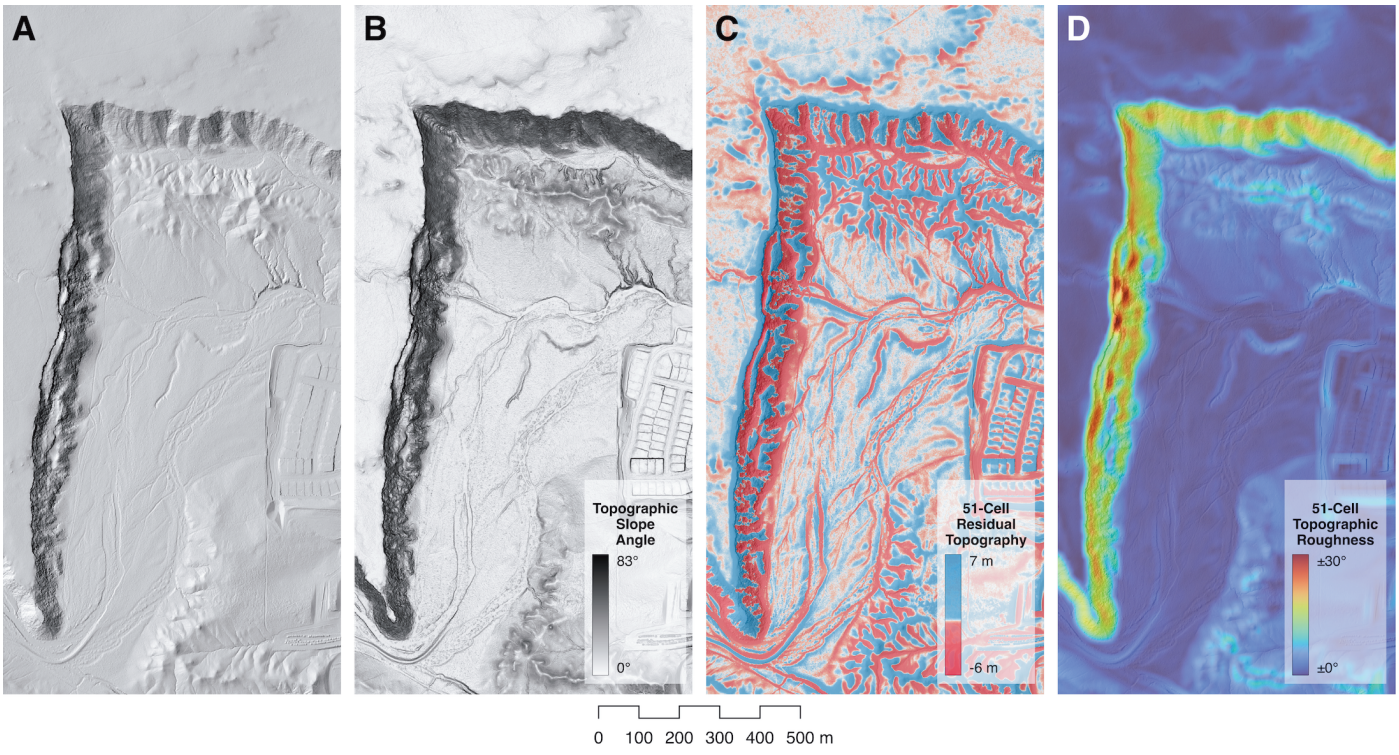


FIGURE 4. Lidar-derived geomorphological visualizations of the SWME. A) Multi-directional hillshade map. B) Slope-shade map. C) 51-cell moving mean residual topographic map. D) 51-cell standard deviation of slope topographic roughness map.

TABLE 2. Probabilistic factor of safety (F) simulation results for 100,000 Monte Carlo iterations.

Model	r_u	Minimum	Maximum	Mean	Mean:Median	Standard Deviation	Prob [$F < 1$]
Vertical Dry	0.00	0.79	1.03	0.91	1.00	±0.03	1.00
Vertical Wet	0.15	0.55	0.73	0.64	1.00	±0.02	1.00
Non-vertical Dry	0.00	1.06	1.43	1.24	1.00	±0.04	0.00
Non-vertical Wet	0.15	0.84	1.14	0.99	1.00	±0.04	0.63

We manually adjusted pore pressure coefficient values to find a threshold value that would produce instability in the non-vertical slope, finding that a value of r_u=0.15 produces a mean factor of safety essentially equal to the critical value of $F = 1$ (and corresponding to a probability of hillslope instability of Prob[$F < 1$] = 0.63). Higher values of r_u would increase the probability of instability.

DISCUSSION

The previously unreported basalt-capped landslides developed along the SWME are examples of rotational mass movements with resistant caprocks, a type originally named Toreva blocks by Reiche (1937) after a type locality near Toreva, Arizona. Others have described extensive Toreva block complexes developed in basalt-capped Santa Fe Group strata along portions of the Rio Grande in northern New Mexico (Reneau and Dethier, 1996; Carrara and Dethier, 1998; Haneberg et al., 2002; Das and Wegmann, 2025). Watson and Wright (1963) and Haneberg (1992) described similar Toreva block landslides in the Chuska Mountains of northwestern New Mexico and along the High Plains escarpment in DeBaca County, New Mexico.

Reiche (1937) and Watson and Wright (1963) inferred that, given the current semiarid climate in New Mexico, the mass movements likely occurred during cooler, wetter periods. Reneau and Dethier (1996) and Dethier and Reneau (1996) dated lake deposits formed behind landslide dams along the Rio Grande in White Rock Canyon and found evidence for at least four episodes of landsliding, damming, and breaching between 17.5 and 12.4 ka (^{14}C dating methods), inferring that the movements were triggered in response to Rio Grande downcutting driven by a combination of glacial and pluvial runoff. Dethier and Reneau (1996) wrote "…late Pleistocene climate changes may have triggered similar mass movements elsewhere in the Southwest." (See, for example, Allen and Anderson, 2000, for a discussion of Pleistocene climate variability in New Mexico). Our surface water flow accumulation map can be interpreted as a generalized proxy for shallow groundwater availability along the SWME, as a measure of the ability of the watershed to deliver surface water to the SWME, or as a combination of the two. It is not clear whether the surface

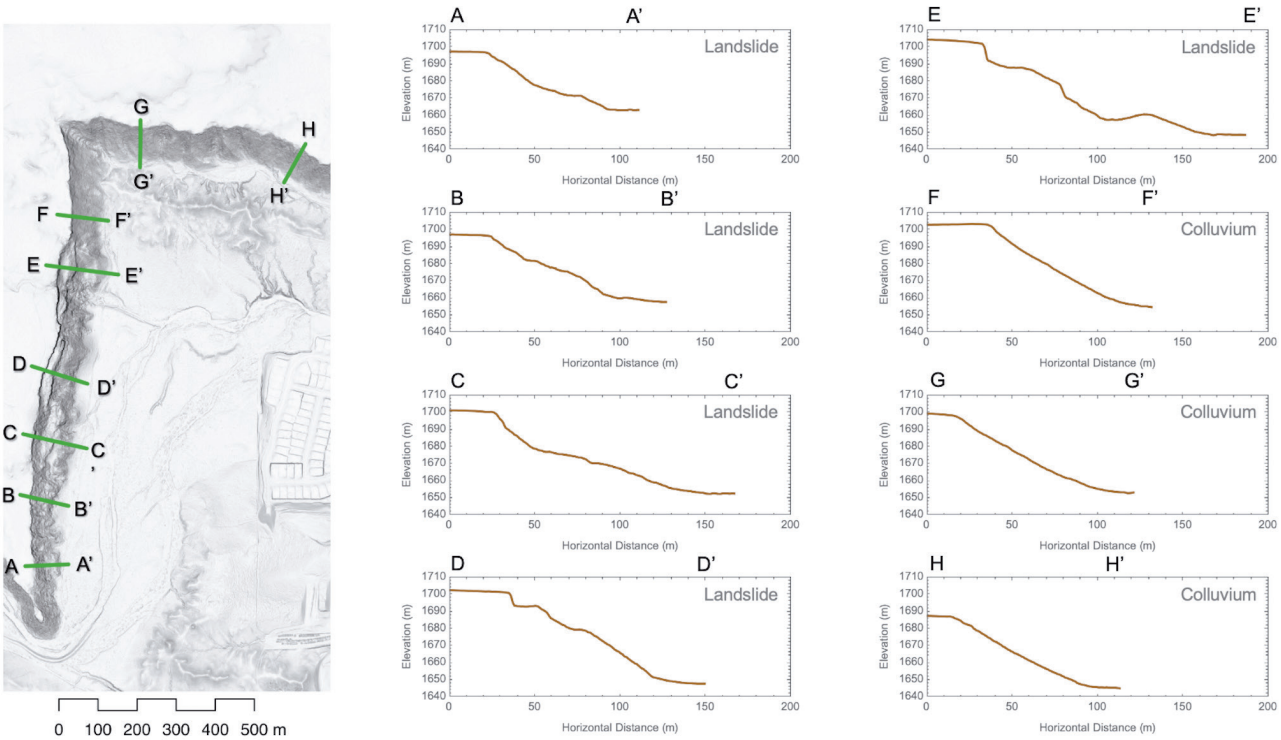


FIGURE 5. Lidar-derived topographic profiles across landslide and non-landslide (colluvium) slopes along the SWME and an adjoining portion of the larger West Mesa escarpment.

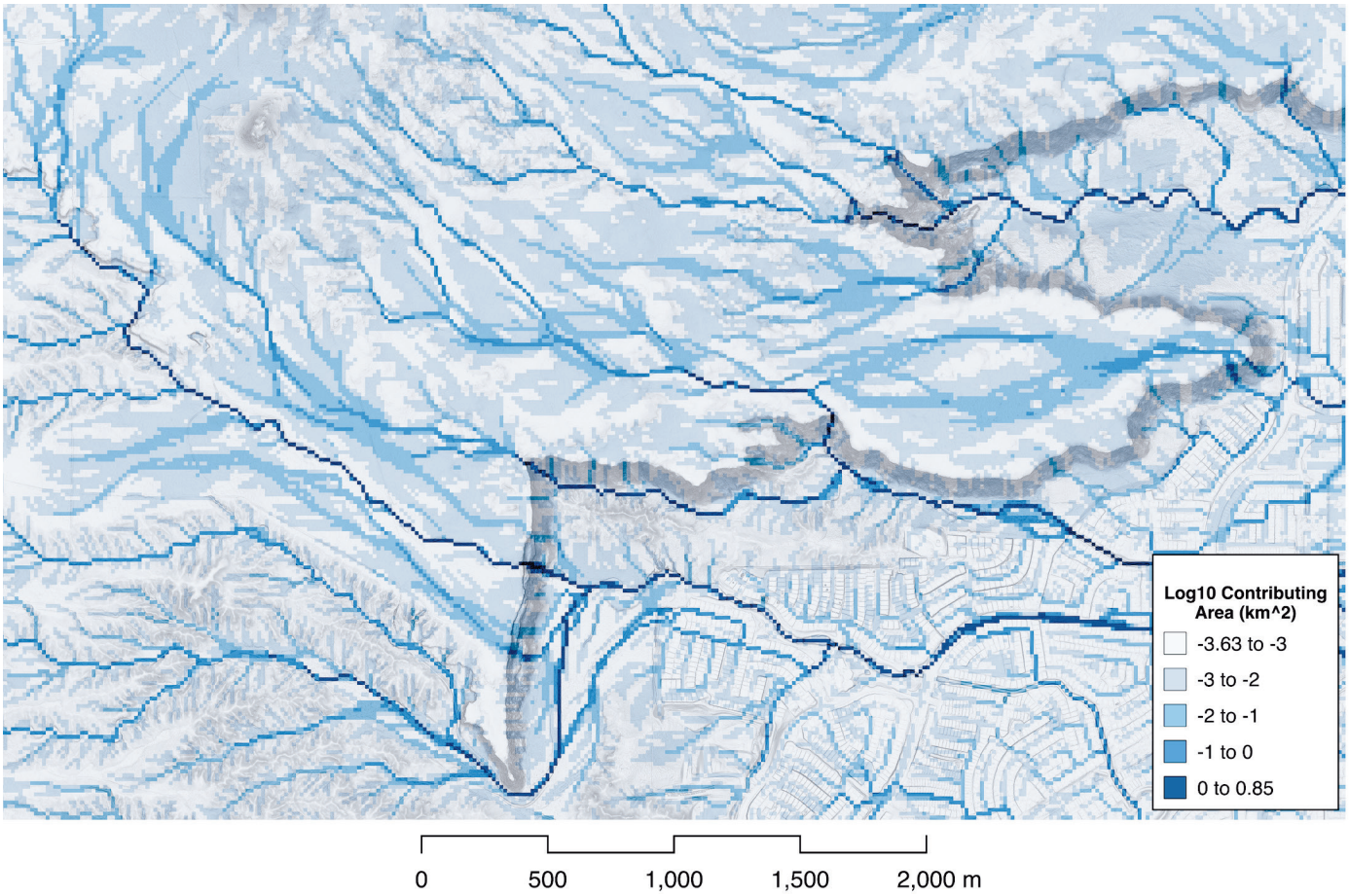


FIGURE 6. Surface water flow accumulation map showing contributing areas across a hydrologically corrected lidar DEM aggregated to 50 m (164 ft) cell size.

and shallow groundwater systems were connected when landsliding occurred; however, we think it is unlikely that the existence of large landslides at a point along the SWME with an unusually large surface drainage area is purely coincidental. In a recently published paper, Das and Wegmann (2025) used Interferometric Synthetic Aperture Radar (InSAR) data collected between 2017 and 2023 to infer continuing line-of-sight Toreva block complex movement on the order of several millimeters per year along the Rio Grande adjacent to Black Mesa, even under Holocene conditions.

The only radiometric age constraint on the age(s) of the SWME landslides is ~218 ka, based on dates of the Albuquerque Volcanoes (Singer et al., 2008), which must predate the landslides. There is currently no obvious field evidence—for example, springs, unusually lush vegetation, or conspicuously fresh earth—of ongoing slope mass movement, and the alluvial fans developed along the base of the escarpment suggest that it is currently being degraded, instead, by removal of fine sediments beneath the basalt blocks. Based on similarities with other Toreva block landslide complexes in New Mexico, it is likely that the SWME landslides likewise occurred during the late Pleistocene.

LaHusen et al. (2016), Booth et al. (2017), and Gariss (2019) combined topographic roughness maps with radiocarbon dates to elucidate the history of movement of landslide complexes in the Pacific Northwest. Haneberg (2008) did not have radiocarbon dates but similarly suggested that roughness maps of a Toreva block landslide along the Rio Grande between Velarde and Pilar, New Mexico, could be used to qualitatively infer the relative recency of landslide activity. As shown in Figure 4, the roughest portions of the SWME correspond to the most

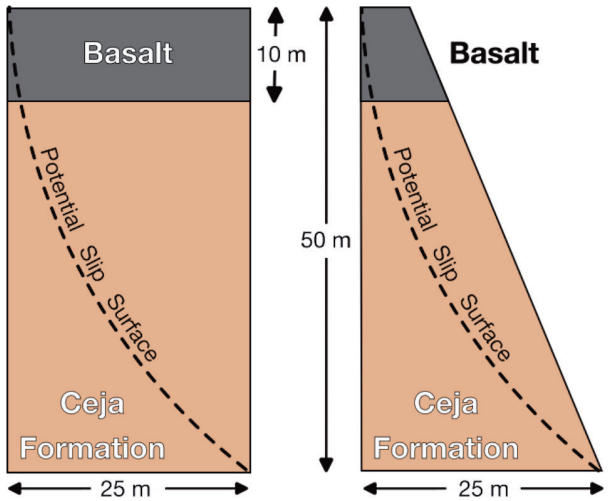


FIGURE 7. Schematic illustrations of the geometry used for probabilistic simulations of idealized vertical (left) and non-vertical (right) slope stability.

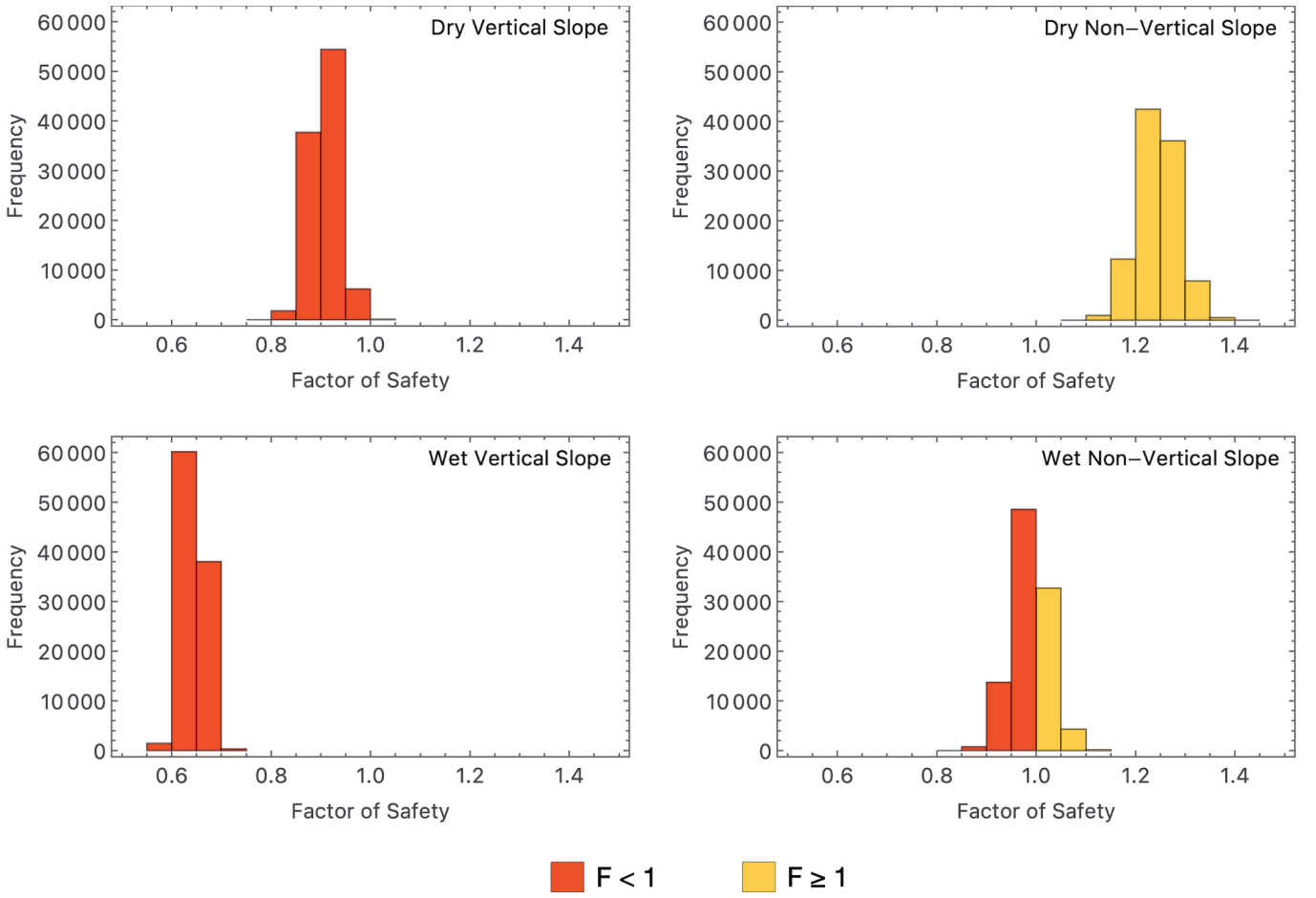


FIGURE 8. Histograms of calculated factors of safety for the four simulated slopes based on 100,000 Monte Carlo iterations. Values of F<1 imply instability (red) and values of F≥1 imply stability (gold). All histograms are plotted using identical ranges to facilitate comparison.

significantly developed landslides. The degree of roughness appears to increase slightly from south to north along the SWME. If the increase is real, it may imply that the landslides occurred sequentially as Ceja Formation material was removed from south to north. This is also consistent with the absence of landslides along the northernmost 300 m (984 ft) or so of the SWME, where it is adjacent to hills underlain by remnants of the Ceja Formation.

The results of our slope stability simulations show that even dry vertical slopes would have been highly susceptible to failure, suggesting that landsliding may have started shortly after lateral support was removed during topographic inversion. Infiltration of surface water into the watershed above the SWME, particularly during the wetter and cooler late Pleistocene pluvial stages, would have greatly increased the likelihood of landsliding (especially if the originally exhumed slopes were not nearly vertical). Although we cannot rule out earthquakes as possible triggers, especially given the proximity of active faults associated with the Albuquerque Volcanoes, they do not appear necessary based on our slope-stability analyses. This contrasts with, for example, some large paleo-landslides studied by Dortch et al. (2009) for which earthquakes may have been necessary to trigger the movement of even fully saturated rock slopes.

The spatial coincidence between the SWME escarpment and an aeromagnetically inferred fault suggests a structural influence on escarpment development, but the nature of that relationship is not well constrained. One scenario, shown on Figure 9, illustrates the evolution of the SWME escarpment in four stages: 1) down-to-the-east displacement along a normal fault produced a fault scarp or monoclinal flexure; 2) subsequent erosion prior to emplacement of the Albuquerque Volcanoes basaltic lava flows may have modified this feature, potentially forming an obsequent fault-line scarp *sensu* Blackwelder (1928); 3) basaltic lava flows terminated against this pre-existing topographic boundary; and 4) later incision, possibly during late Pleistocene pluvial conditions, generated steep slopes that subsequently failed by landsliding.

This interpretation requires conditions that are not directly demonstrated in the field area, including a substantial contrast in erodibility across the fault and geomorphic conditions capable of preserving a west-facing scarp despite inferred eastward paleodrainage. Thus, this conceptual model should be regarded as non-unique and speculative. Alternative explanations include structural control on erosion without full topographic inversion, subtle lithologic variability within the Ceja Formation, or coincidence between the escarpment and aeromagnetic lineation, none of which can be ruled out with the available data.

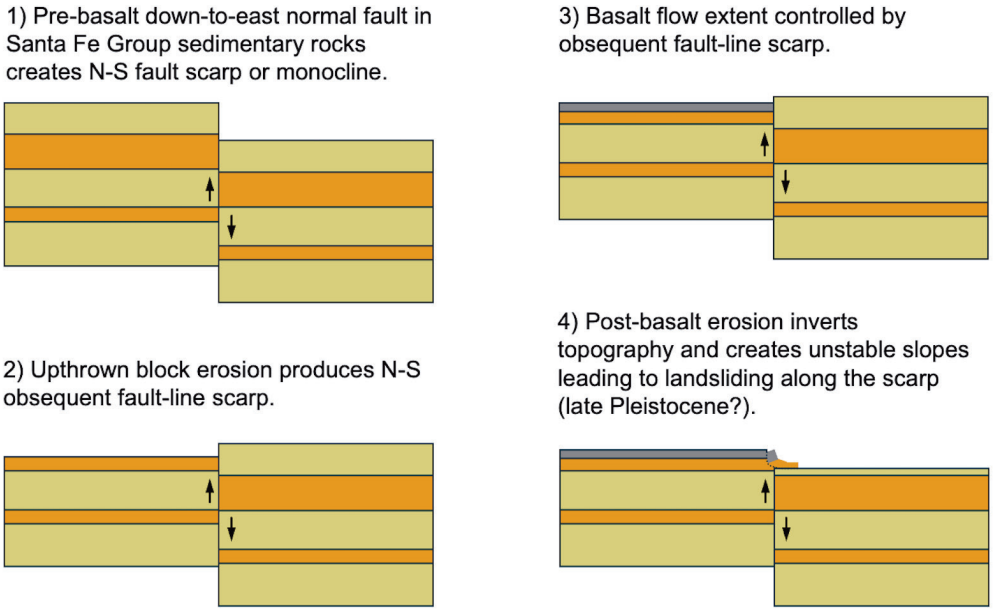


FIGURE 9. Schematic cross-sections illustrating a speculative four-step geomorphological history of the SWME escarpment.

Our interpretation relies on interpretations of down-to-the-east displacement across a projected fault (e.g., Connell, 2008). It is possible that north of the Don #1 well, the western fault with down-to-the-west separation becomes dominant, as suggested by Shroba et al. (2003), or that localized structural or geomorphic complexities influenced lava flow pathways. We find no clear supporting evidence for these alternatives in available outcrops or lidar data. Given the limited exposure of the Ceja Formation, it is also possible that the alignment between the escarpment and aeromagnetic anomaly is coincidental. Regardless of specific mechanisms, the linearity of the SWME escarpment and its association with a mapped geophysical feature suggest that structural influences likely played a role in the development of this linear feature, even if the details of that relationship remain poorly resolved.

Although the SWME landslides, which are in a lightly visited portion of a natural area within the Petroglyph National Monument, are unlikely to be threatened by development and do not pose a hazard to life or property, they are interesting landforms that raise questions about and perhaps shed light on the evolution of an anomalous portion of the West Mesa escarpment. High-resolution drone lidar terrain modeling, supported by ^{14}C dating of organic material from sediments accumulated behind back-tilted Toreva blocks, or by cosmogenic ^{36}Cl dating of dislodged basalt blocks, may be a fruitful direction for future research. Interferometric Synthetic Aperture Radar (InSAR) analysis (e.g., Das and Wegmann, 2025) or repeated lidar surveys (e.g., Johnson et al., 2023) may also be useful to confirm the current state of inactivity.

DATA AVAILABILITY

The lidar coverage we used for this work is freely available through the U.S. Geological Survey National Map download client (https://apps.nationalmap.gov/downloader/#/).

ACKNOWLEDGEMENTS

Mr. Forest Replogle facilitated the transfer of Mid-Region Council of Governments lidar coverage at the start of Haneberg's work on the SWME. Reviews and comments by Paul Santi and Karl Wegmann helped to improve the manuscript. We are also deeply indebted to our friend and colleague John Hawley for innumerable, lengthy discussions over the decades about New Mexico geology, including the SWME.

REFERENCES

Allen, B.D. and Anderson, R.Y., 2000, A continuous, high-resolution record of late Pleistocene climate variability from the Estancia basin, New Mexico: Geological Society of America Bulletin v. 112, no. 9, p. 1444–1458. https://doi.org/10.1130/0016-7606(2000)112<1444:ACHRRO>2.0.CO;2

Atlantic, 2018, Project Report, Mid-Region Council of Governments (MRCOG)–New Mexico, 18001. Online resource available at https://prd-tnm.s3.amazonaws.com/StagedProducts/Elevation/metadata/NM_MRCOG_2018_C20/NM_MRCOG_B1_2018/reports/18001_ProjectReport.pdf (Accessed January 2026).

Bishop, A.W., 1955, The use of the slip circle in the stability analysis of slopes: Geotechnique, v. 10, p. 129–150. https://doi.org/10.1680/geot.1955.5.1.7

Blackwelder, E., 1928, The recognition of fault scarps: Journal of Geology, v. XXXVI, no. 4, p. 289–311. https://doi.org/10.1086/623519

Booth, A.M., LaHusen, S.R., Duvall, A.R. and Montgomery, D.R., 2017, Holocene history of deep-seated landsliding in the North Fork Stillaguamish River valley from surface roughness analysis, radiocarbon dating, and numerical landscape evolution modeling: Journal of Geophysical Research Earth Surface, v. 122, no. 2, p. 456–472. https://doi.org/10.1002/2016JF003934

Carrara, P.E. and Dethier, D.P., 1998, Preliminary map of landslide deposits in the Los Alamos 30' x 60' quadrangle, New Mexico: U.S. Geological Survey Miscellaneous Field Studies Map 2328, scale 1:100,000. https://doi.org/10.3133/mf2328

Connell, S.D., 2006, Preliminary geologic map of the Albuquerque-Rio Rancho Metropolitan Area and vicinity, Bernalillo and Sandoval Counties, New Mexico: New Mexico Bureau of Geology and Mineral Resources, Open-file Report 496, 2 pl, GIS dataset. https://doi.org/10.58799/OFR-496

Connell, S.D., 2008, Geologic map of the Albuquerque-Rio Rancho metropolitan area and vicinity, Bernalillo and Sandoval Counties, New Mexico: New Mexico Bureau of Geology and Mineral Resources, Geologic Map 78, scale 1:50,000. https://doi.org/10.58799/GM-78

Connell, S.D., Smith, G.A., Geissman, J.W., and McIntosh, W.C., 2013, Climatic controls on nonmarine depositional sequences in the Albuquerque Basin, Rio Grande rift, north-central New Mexico, *in* Hudson, M.R., and Grauch, V.J.S., eds., New Perspectives on Rio Grande Rift Basins: From Tectonics to Groundwater: Geological Society of America Special Paper 494, p. 383–425. https://doi.org/10.1130/2013.2494(15)

Das, R. and Wegmann, K.W., 2025, InSAR characterization of short-term deformation in a Late Quaternary landslide complex in the lower Rio Grande Gorge, New Mexico, USA: Scientific Reports, v. 15, no. 1, article 21360. https://doi.org/10.1038/s41598-025-98062-4

Dethier, D. P. & Reneau, S. L., 1996, Lacustrine chronology links late Pleistocene climate change and mass movements in northern New Mexico: Geology, v. 24, p. 539–542. https://doi.org/10.1130/0091-7613(1996)024<0539:LCLLPC>2.3.CO;2

Dortch, J.M., Owen, L.A., Haneberg, W.C., Caffee, M.W., Dietsch, D., and Kamp, U., 2009, Nature and timing of large landslides in the Himalaya and Transhimalaya of northern India: Quaternary Science Reviews, v. 28, no. 11-12, p. 1037–1054. https://doi.org/10.1016/j.quascirev.2008.05.002

Garriss, R.N., 2019, Modeling Surface Roughness as an Indicator of Age and Landslide Susceptibility, and the Spatial Inventory of Prehistoric Landslides: Green River Valley, Washington [unpublished M.S. Thesis]: Portland State University, Paper 5175, 79 p. https://doi.org/10.15760/etd.7051

Gellis, A.C., 1995, Erosion assessment at the Petroglyph National Monument area, Albuquerque, New Mexico: US Geological Survey, Water-Resources Investigations Report 94-4205, 39 p. https://doi.org/10.3133/wri944205

Grauch, V.J.S., Hudson, M.R., and Minor, S.A., 2001, Aeromagnetic expression of faults that offset basin fill, Albuquerque basin, New Mexico: Geophysics, v. 66, no. 3, p. 707–720. https://doi.org/10.1190/1.1444961

Grohmann, C.H., Smith, M.J., Riccomini, C., 2011, Multi-scale analysis of topographic surface roughness in the Midland Valley, Scotland: IEEE Transactions on Geoscience and Remote Sensing, v. 49, p. 1,200–1,213. https://doi.org/10.1109/TGRS.2010.2053546

Haneberg, W.C., 1992, Geologic hazards in New Mexico–Part 2: New Mexico Geology, v. 14, p. 45–52. https://doi.org/10.58799/NMG-v14n3.45

Haneberg, W.C., 1999, Effects of valley incision on the subsurface state of stress—theory and application to the Rio Grande valley near Albuquerque, New Mexico. Environmental & Engineering Geoscience, v. 5, no. 1, p. 117–131. https://doi.org/10.2113/gseegeosci.V.1.117

Haneberg, W.C., 2008, Revisiting an old project with new technology—digital terrain modeling and multi-layered virtual geologic hazard mapping along a proposed highway realignment, Rio Grande gorge, New Mexico: Proceedings, 59th Highway Geology Symposium, May 6–9, 2008, Santa Fe, New Mexico, paper 5.2, 21 p.

Haneberg, W.C., Bauer, P.W., and Chávez, W.X., Jr., 2002, Multilevel geologic hazard assessment mapping in the Rio Grande gorge, northern New Mexico, USA, *in* Bobrowsky, P.T., ed., Geoenvironmental Mapping: Method, Theory and Practice: A.A. Balkema, p. 75–91. https://doi.org/10.1201/9781003761259-5

Johnson, S.E., Haneberg, W.C., Bryson, L.S., and Crawford, M.M., 2023, Measuring ground surface elevation changes in a slow-moving colluvial landslide using combinations of regional airborne lidar, UAV lidar and UAV photogrammetric surveys: Quarterly Journal of Engineering Geology and Hydrogeology, v. 56, no. 2. 15 p. https://doi.org/10.1144/qjegh2022-078

Johnson, S.E. and Haneberg, W.C., 2025, Machine learning for surficial geologic mapping: Earth Surface Processes and Landforms, v. 50, no. 1, p. 1–21. https://doi.org/10.1002/esp.6032

Kelley, V.C., 1977, Geology of the Albuquerque basin, New Mexico: New Mexico Bureau of Geology and Mineral Resources, Memoir 33, 59 p. https://doi.org/10.58799/M-33

LaHusen, S.R., Duvall, A.R., Booth, A.M. and Montgomery, D.R., 2016, Surface roughness dating of long-runout landslides near Oso, Washington (USA), reveals persistent postglacial hillslope instability: Geology, v. 44, no. 2, p. 111–114. https://doi.org/10.1130/G37267.1

Lindsay, J. B., 2016, Whitebox GAT: A case study in geomorphometric analysis: Computers & Geosciences, v. 95, p. 75–84. https://doi.org/10.1016/j.cageo.2016.07.003

Lindsay, J.B. and Dhun, K., 2015, Modelling surface drainage patterns in altered landscapes using LiDAR: International Journal of Geographical Information Science, v. 29, no. 3, p. 397–411. https://doi.org/10.1080/13658816.2014.975715

[NPS] National Park Service, 1991, Land Protection Plan, Petroglyph National Monument: National Park Service and the City of Albuquerque, New Mexico, 34 p.

Peate, D.W., Chen, J.H., Wasserburg, G.J., Papanastassiou, D.A. and Geissman, J.W., 1996, $^{238}U/^{230}Th$ dating of a geomagnetic excursion in Quaternary basalts of the Albuquerque Volcanoes Field, New Mexico (USA): Geophysical Research Letters, v. 23, no. 17, p. 2271–2274. https://doi.org/10.1029/96GL02064

Personius, S.F., and Jochems, A.P., compilers, 2016, Fault number 2049, unnamed faults near Albuquerque Volcanoes, in Quaternary fault and fold database of the United States: U.S. Geological Survey, https://earthquakes.usgs.gov/hazards/qfaults (accessed January 2026).

Reiche, P., 1937, The Toreva-Block: A distinctive landslide type: Journal of Geology, v. 45, no. 5, p. 538–548. https://doi.org/10.1086/624563

Reneau, S.L. and Dethier, D.P., 1996, Late Pleistocene landslide-dammed lakes along the Rio Grande, White Rock Canyon, New Mexico: Geological Society of America Bulletin, v. 108, no. 11, p.1492–1507. https://doi.org/10.1130/0016-7606(1996)108<1492:LPLDLA>2.3.CO;2

Singer, B.S., Jicha, B.R., Kirby, B.T., Geissman, J.W., and Herrero-Bervera, E., 2008, $^{40}Ar/^{39}Ar$ dating links Albuquerque Volcanoes to the Pringle Falls excursion and the Geomagnetic Instability time scale: Earth and Planetary Science Letters, v. 267, p. 584–595. https://doi.org/10.1016/j.epsl.2007.12.009

Shroba, R.R., Thompson, R.A., Schmidt, D.L., Personius, S.F., Maldonado, F., and Brandt, T.R., 2003, Geologic map of the La Mesita Negra SE quadrangle, Bernalillo County, New Mexico: U.S. Geological Survey Miscellaneous Field Studies Map MF-2416, scale 1:24,000. https://doi.org/10.3133/mf2416

Sweeney, R.E., Grauch, V.J.S., and Phillips, J.D., 2002, Merged digital aeromagnetic data for the Middle Rio Grande and Southern Española basins, New Mexico: U.S. Geological Survey Open-file Report 02-205, 15 p. https://doi.org/10.3133/ofr02205

Tarboton, D. G., 1997, A new method for the determination of flow directions and upslope areas in grid digital elevation models: Water Resources Research, v. 33, no. 2, p. 309–319. https://doi.org/10.1029/96WR03137

Watson, R. A., and Wright, H. E, Jr., 1963, Landslides on the east flank of the Chuska Mountains, northwestern New Mexico: American Journal of Science, v. 261, p 525–548. https://doi.org/10.2475/ajs.261.6.525